An exploration of the deformability behaviours dominated by braiding angle during the forming of the triaxial carbon fibre braids

Shenglei Xiao, Peng Wang, Damien Soulat, Hang Gao

Version of Record: https://www.sciencedirect.com/science/article/pii/S1359835X20301287
Manuscript_8051760abaf2cf8bdfa84c01796f0a5a

An exploration of the deformability behaviour dominated by braiding angle during the forming of the triaxial carbon fibre braids

Shenglei Xiao [1, 2], Peng Wang [3,4,*], Damien Soulat [2], Hang Gao[1]

[1] *Key Laboratory for Precision and Non-traditional Machining Technology of Ministry of Education, School of Mechanical Engineering, Dalian University of Technology, Dalian, 116024, China*

[2] *University of Lille, Ensait, Gemtex, F-59000 Roubaix, France*

[3]*University of Haute-Alsace, Ensisa, Lpmt, F-68000 Mulhouse, France*

[4]*University of Strasbourg, France*

* Corresponding author. Tel.: +33 3 89 33 66 48. Fax.: +33 3 89 33 63 39

E-*mail address*: peng.wang@uha.fr

Abstract

The present study focuses on the experimental and analytical analysis of the deformability behaviour of the triaxial braided fabrics during forming. The mechanical model of the yarns based on the parameters of the reinforcements and the forming process was discussed. On the other hand, the geometric model related to the braiding angle was proposed to describe the yarns and the reinforcement deformations and to predict the yarns sliding. From the geometric model, the in-plane shearing and the material draw-in could also be predicted with respect to its magnitude and location on the braided fabric. It is clearly deduced from this study that the variation of deformability behaviours is directly impacted by the braiding angle, which is the crucial parameter for the braided fabrics.

Keywords: A. Fabrics/textiles; E. Forming; Braided reinforcement; Braiding angle

1. Introduction

In manufacturing the composites with complex shapes, the Liquid Composite Moulding (LCM) process provides reliable performances with respect to repeatability, high production rate and low final cost [1]. As the first stage of LCM, the preforming process that the dry reinforcements are rapidly deformed into the ideal shape before resin infusion is crucial to ensure the quality of the composites. It is not only impacted by the processing machine or parameters [2,3], but also decided by reinforcements characteristics. The braided fabrics as promising composite reinforcements have higher levels of conformability, drapability, torsional and structural integrity, which makes it possible to produce composite structures with intricate geometries to the near-net-shape [4]. For example, the complex shapes of braided fabric as diamond and cone can be implemented during the braiding process resort to a CAD model both externally and internally [5]. Moreover, braiding process using specific rules, "topological" way in algorithms and software, make the braiding structures being visualized in 3D, and optimized in the same way as it is already possible for woven structures [6]. As one type of braided fabrics, the triaxial fabrics, which contain the axial yarns added along the longitudinal axis as third yarn direction, could effectively enhance the high fibre volume fraction for mechanical application [7]. Therefore, the braided fabrics are getting more interests in their mechanical properties that are also basic knowledge for understanding deformability behaviours of fabrics during preforming process [8,9] .

Reinforcements preforming process is a difficult stage that contains the complex deformability behaviours influenced by many factors including forming load, tools shape, properties of yarn and fabric [10]. The deformability behaviours decided by the mechanical properties of the fabric, such as in-plane shearing and material draw-in, directly determine the various forming defects [11]. The wrinkling, one of the common forming defects, is dependent on the co-effect of in-plane shearing and bending [12], and has been studied by

previous researchers using the finite element and experimental analysis to figure out the impact from processing parameters [11,13], and try to optimize them to avoid such defect [14,15]. The material draw-in also locally generates concentration of fibre density around the preforming shape [16], negatively impacting the performance of the composites. As another deformability behaviour, the yarns sliding or inter-ply sliding could probably induce a decrease in local fibre density, or buckles on the surface of preforming shape, producing the inhomogeneous resin impregnation [2,17].

Accordingly, the precisely describing of characteristics of deformability behaviours is essential to acquire the ideal mechanical properties of composites. Unfortunately, by now, the research work mainly focuses on the preforming of woven fabrics and trying to connect the processing parameters, such as blank-holder pressure and tools shape [16,18], with the law of characterizations of deformability behaviours. The studies on preforming of braided fabrics are relatively scarce, and the basic braiding parameters associated with deformability behaviours, especially braiding angle, are short of sufficient attention. In fact, the braiding angle, as the specific parameter of braided fabrics compared to woven ones, could be changed exactly as required that the mechanical properties of braided composite parts are also directly influenced. The high degree of correlations between vibration behaviours and braiding angles can be found in [19]. And the ability of energy abortion is also enhanced as combining the fabrics with braiding angle 30°, with the presence of flexible resins [20]. Besides, the tensile strength, modulus and Poisson ratio decrease significantly with increasing the braiding angle [21]. Thus, it is confirmed that the variation of the braiding angle effectively impacts the final performance of braided composites. In the manufacturing of composites with complex shapes, the deformability behaviours during preforming could be greatly related to composites performance. It is thus reasonable to believe that the braiding angle would impact the deformability behaviours. However, the exploration of the variation of deformability

behaviours changed by braiding angle during preforming is still absent and needs to be quantitatively analysed in order to make them predictable before preforming. Besides, during the preforming process, the yarns would be deformed into the desired shape, thus the mechanical model of yarn needs to be analysed in mesoscale based on the basic parameters including processing and reinforcements parameters. Especially for the yarn tension, which is generated during preforming process and the root driven force for yarns sliding. Although Ref.[22] proposed the tension model of yarn during woven fabrics preforming, the braided fabrics would show large difference because the braiding angle decides the yarns position relative to a fixed punch tool. Unfortunately, such mechanical analysis of yarns for braided fabrics during preforming is also absent.

Therefore, in this study, the deformability behaviours during preforming process of triaxial braided fabrics such as in-plane shearing, yarn sliding or even material draw-in will be originally investigated with respect to their magnitude and location based on the different braiding angles. The tension model of the yarns related to braiding angle during preforming will be proposed based on braiding angle and punch tool parameters. And then, the geometrical analysis for yarns sliding and in-plane shearing is also proposed and verified.

2. Experimental details

The triaxial fabrics with different braiding angles were made by the continuous carbon yarns through the overbraiding process. After overbraiding process, the triaxial braid presents the tubular type, which needs to be cut carefully in order to obtain the single-layer tested fabric as shown in Fig. 1a. The directions of fabric are also defined, the axial direction (X) and transversal direction (Y). The characteristics of tested fabric are presented in Table. 1. The braiding angle $\beta/2$ is defined as half of interlaced angle β. During preforming, the in-plane shearing would take place. The interlaced yarns rotate towards each other along the axial direction, hence the interlaced angle β would be changed into α, as shown in Fig. 1b.

The shearing angle γ, which is a classical and positive definition that directly indicates the extent of in-plane shearing, can be expressed as:

$$\gamma = \beta - \alpha \tag{1}$$

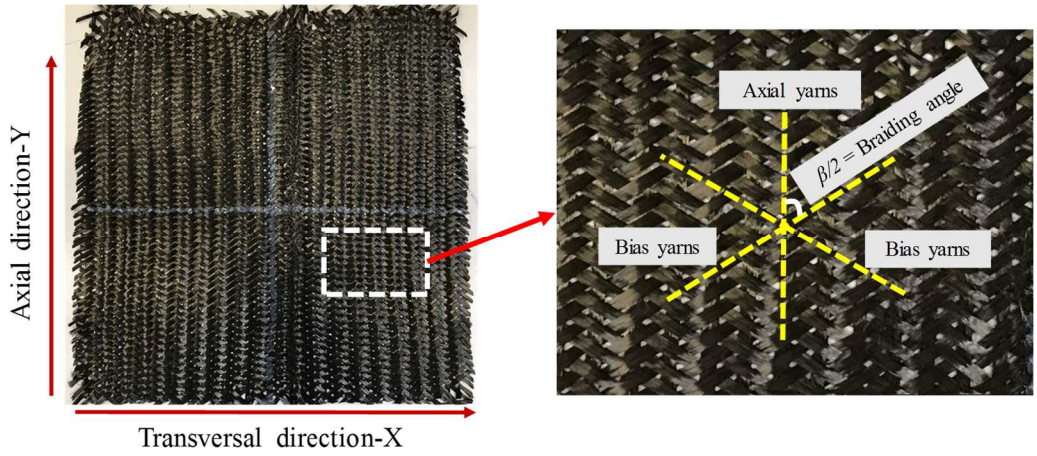

(a)

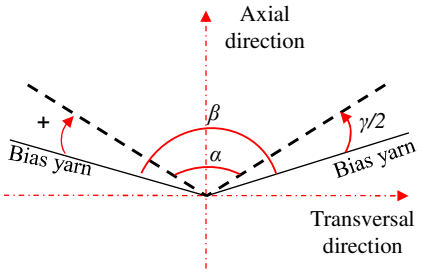

(b)

Fig. 1. Triaxial braided fabric with notifications; (a) The structure of the triaxial braid, (b) the classical definition of shearing angle.

Table 1
The main characteristics of tested braids

Parameters	Value
Yarns	792 tex
Area density (g/m^2)	510 ± 5
Thickness d (mm)	2.37
Braiding angle $\beta/2$ (°)	30; 55; 65
Number of yarns per cm	3.9
Fabric area A (mm^2)	280×280
Yarn width w (mm)	4.0
The distance between two adjacent axial yarns-L_0 (mm) (centre to centre)	7.5±0.5
The distance between two adjacent bias yarns-L'_0 (mm) (centre to centre)	4.0±0.5

The preforming machine used in these tests is shown in Fig. 2. The blank-holder jointed with the pneumatic jack provides the blank-holder pressure on the upper plate. The upper plate is moveable so that test fabrics can be placed with desired orientation between the upper plate and die. The die is fixed on the machine and is made by the same material with upper plate, Plexiglas. The punch tool was selected hemisphere shape with 150 mm diameter, which is driven by the special pneumatic jack with constant speed 45 mm/min. The upper plate and die have the circular holes with 160 mm diameter in their centre where punch tool could go across, thus the fabrics could be deformed. To further guarantee the preforming successfully, the corner at the base of the hole in the upper plate is produced. In this circumstance, the centre of punch tool and braided fabric are coincident during preforming. The blank-holder pressure was constant in all the tests, but the braiding angle was varied as shown in Table. 1. There were at least three tests for each braiding angle in order to ensure the results available.

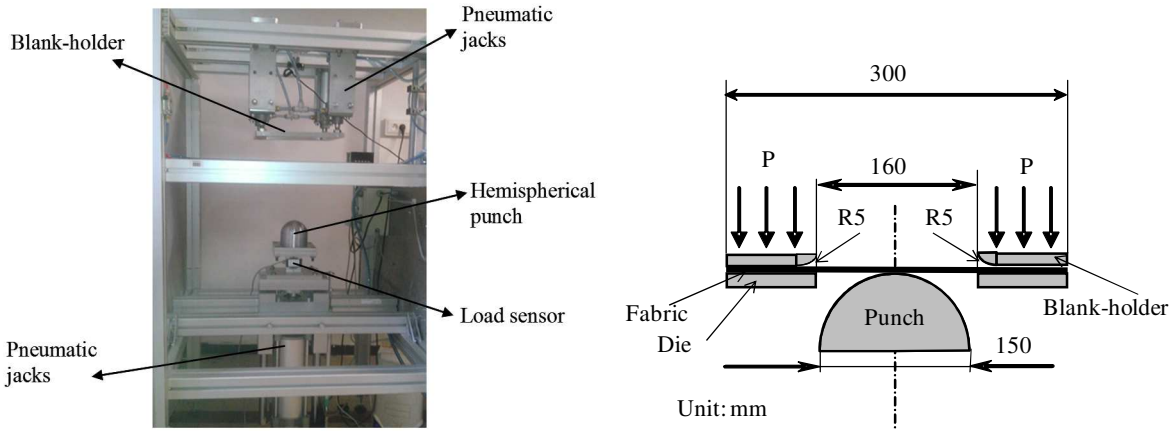

Fig. 2. The preforming machine.

Before preforming, the yarns which locate into punch zone sustaining the out-of-plane bending during preforming were numbered in order to conveniently analyse deformability behaviour. Firstly, the two centre lines of fabric, as well as punch tool, I and II lines are defined (see Fig. 3), which align along with axial and transversal directions across centre point of fabric and punch tool. It is clearly seen that axial yarns align symmetrically along I line. Secondly, The axial yarn across the centre of punch tool is considered as N°0, and the

other axial yarns that locate into punch zone along the transversal direction of fabric can be numbered N°i as shown in Fig. 3. Hence, the distance between N°0 and N°i can be expressed as iL_0, L_0 is the distance between two adjacent axial yarns as shown in Tab. 1. By contrast, the bias yarns except the one across the centre of punch tool, are not symmetrical along I and II lines. Thus, numbering the bias yarns should be along their aligned direction as shown in Fig. 3. The bias yarn across the centre of punch tool is considered as N°0, and the other bias yarns that locate into punch zone can be numbered N°i as shown in Fig. 3.

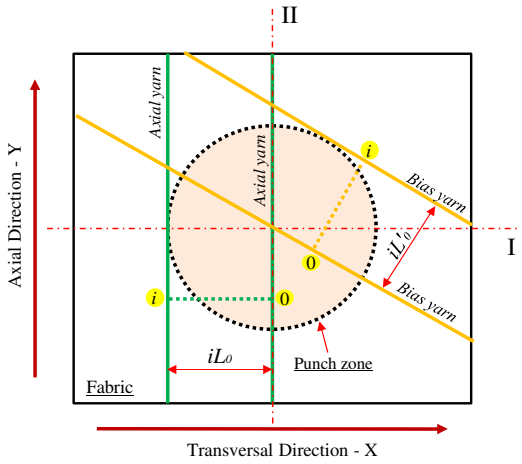

Fig. 3. The axial and bias yarns numbered before preforming.

Before demoulding (blank-holder moving back), the deformed fabrics had been fixed using the settling agent in order to avoid the elastic spring-back. A video camera installed on the device and linked with a computer was used to monitor preforming process and measure the evolution of yarn sliding. After the consolidation of the settling agent, the blank-holder moved back to the original position and the deformed fabric was moved outside from the device for further measurement.

3. Preforming results

The deformability behaviours such as in-plane shearing, material draw-in and yarns sliding can be noted during preforming. In order to clearly present the characteristics of deformability behaviours varied with braiding angles, yarns sliding zones were objectively contoured by white lines on the fabrics after tests, and the corresponding figure aimed to point out

deformability behaviours was also drawn, as shown in Fig. 4. Fig. 4a shows the preformed fabric with small braiding angle 30°, it is visible that material draw-in, in-plane shearing and yarns sliding zones are almost symmetrical along the I line. The in-plane shearing takes place along the II line out of punch zone, where the material draw-in also occurs, thus the in-plane shearing angle is positive according to the definition as described in Section 2. The contour line of bias yarns sliding zones is profiled as a parabola, which, in particular, shows uneven sliding at the ends of bias yarn. This is because the bias yarns are not symmetrical along neither I nor II line.

As increasing braiding angle to 55° (see in Fig. 4b), the differences in behaviours presentation can be observed. The identical axial yarns sliding at the ends, showing symmetrical distribution along I, takes place of material draw-in as shown in braiding angle 30°. Besides, the in-plane shearing takes place along I line, and as the positive definition of shearing angle in section 2, yet the shearing angle in braiding angle 55° shows negative value. This is because the interlaced bias yarns rotate outwards against the defined axial direction. Furthermore, although uneven sliding of bias yarns at the ends is still observed, the sliding zones are symmetrical along II, which is different from braiding angle 30°.

Further increasing the braiding angle to 65° as shown in Fig. 4c, the identical axial yarns sliding zones are also symmetrical along I. The bias yarns sliding zones also locate symmetrically along II, but the extent of uneven sliding becomes smaller than that in 30° and 55°. In-plane shearing also takes place along I, presenting the negative value of the shearing angle. But the material draw-in with a small degree is also observed in the same location. Thus, it can be deduced that the material draw-in, which can be defined as yarns absence in the local fabric after preforming, can be explained by the co-effect of in-plane shearing and yarns sliding that the former takes place at first, then the latter occurs.

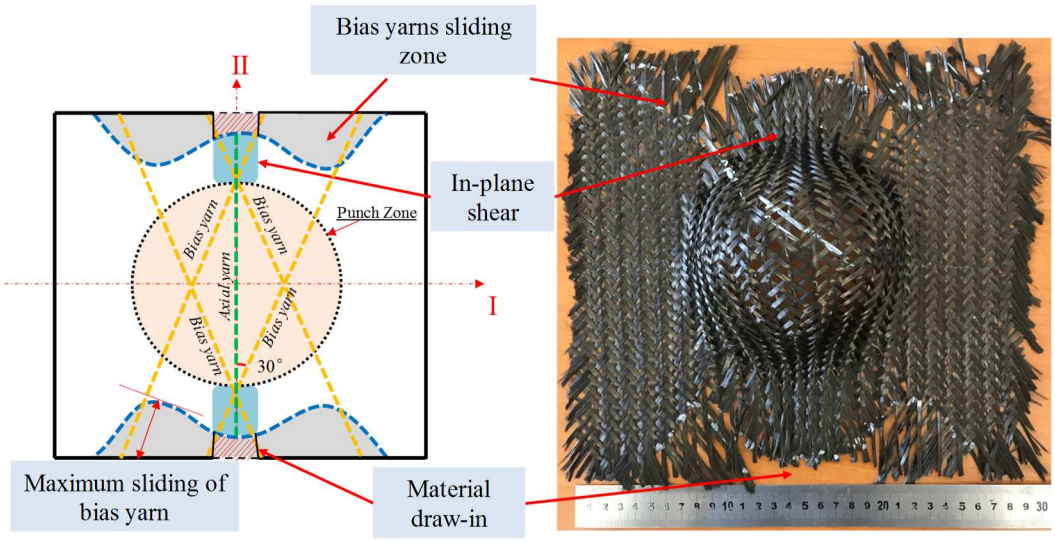

(a) Braiding angle $\beta/2$=30°

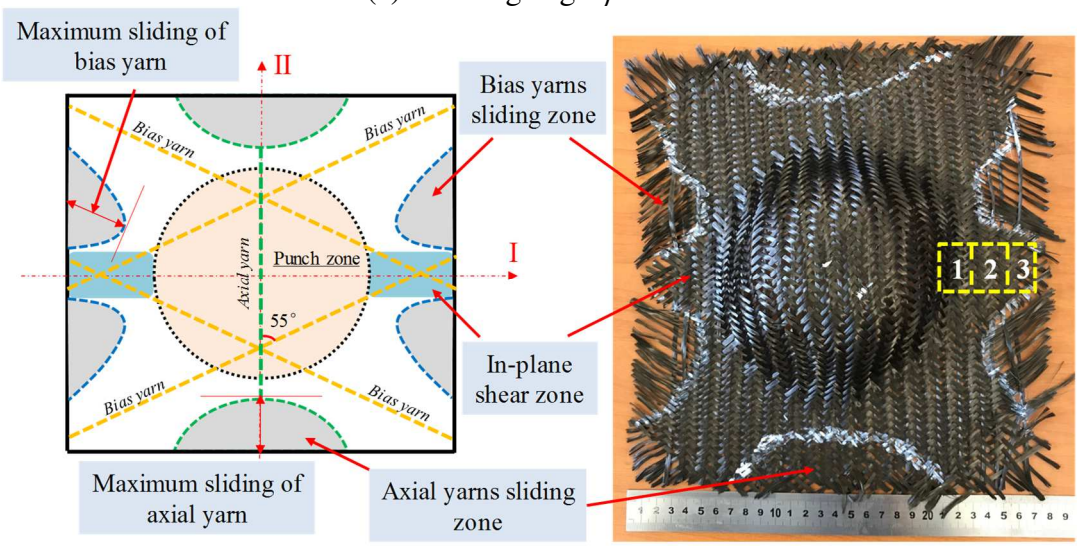

(b) Braiding angle $\beta/2$=55°

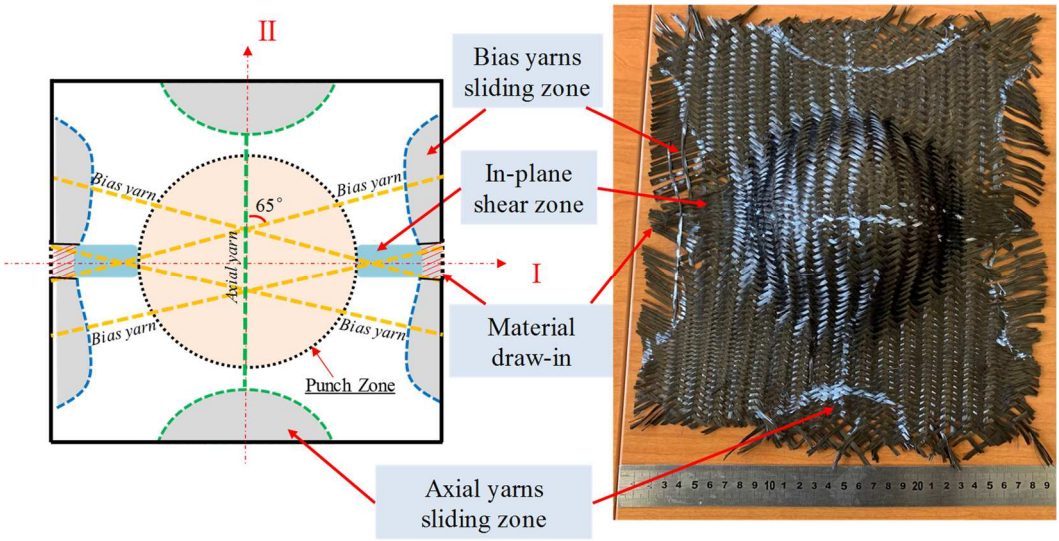

(c) Braiding angle $\beta/2$=65°

Fig. 4. The experimental results performed by different braiding angles.

Consequently, according to the experimental results, it is induced that varied braiding angle can actually influence the appearances of different kinds of behaviours during preforming braided fabrics, including the magnitude and location. The in-plane shearing is no more symmetrical with warp and weft directions simultaneously as shown in woven fabric [23]. Moreover, the excessive yarns sliding and in-plane shearing could directly impact composites quality due to nonhomogeneous fibre density [2].

4. Analysis and discussion

4.1 The mechanical model of yarns deformation

As results discussed above, it is clearly suggested the deformability behaviours present the difference in appearance with varied braiding angles. The in-plane shearing and yarns sliding out of punch zone are generated by tension of yarn during preforming. In order to explore the deformability behaviours, the mechanical analysis of the yarns deformation should be clear at first. Besides, according to the structure of triaxial fabrics, the axial and bias yarn should be analysed respectively.

As shown in Fig. 5, The N°i axial yarn is symmetrical along I line, O is the central point of punch tool and fabric. R is the radius of punch tool, in theory, it is roughly equal to the radius of punch zone. If the traction force along punch tool surface during preforming is ignored, the vertical distance between O point and N°i axial yarn would be fixed and calculated as iL_0 before and after preforming, L_0 is shown in Tab. 1. Since N°i axial yarn that is driven by punch tool sustains the out-of-plane bending during preforming, and it is symmetrical along I line. Thus, it can be projected into half Z-Y plane as shown in Fig. 5b, Z is the punch direction, O$'$ is the corresponding centre point of half-circle deformed by N°i axial yarn during preforming. Thus, N°i axial yarn deformed during preforming can be naturally divided into two portions. The first portion, the yarn segment AE in Fig. 5, continually deforms within punch zone, making a displacement in Z direction. The point A stands for the vertex of

deformed circle by corresponding N°i axial yarn, point M represents the yarn beginning to contact the punch tool surface. The θ_i^A expresses the angle of the yarn/punch contact area from point A to M. The portion of yarn QE portrays the contact area between the yarn and corner of upper plate. During the preforming process, indeed, the first portion AE does not contact the entire punch tool surface, as the yarn segment MQ without contacting any surface of punch tool. The second portion of yarn is segment yarn ET, which is located between upper plate and die, subject to the blank-holder pressure. Due to the first portion of yarn AE driven by punch tool, the tension is generated. When it overcomes the static friction, which is resulted by upper plate and die, and proportional to the length of second portion of yarn ET, the sliding is thereby produced at the ends of yarn as shown in Fig. 5a and 5b, one end slides gradually from the point T to F. During the preforming, the length of segmental yarn AM increases from the onset of preforming process. Accordingly, θ_i^A increases from zero to the maximum value at the end of preforming process as shown in Fig. 5b. By contrast, the length of segment yarn MQ decreases. It is clearly acquired that θ_i^A is proportional to the punching displacement in Z direction as well as the sliding at two ends of yarn. At the end of the preforming process, the maximum value of θ_i^A and punching displacement that can be symbolized as r_i^A are attained, as shown in Fig. 5b. The maximum punching displacement r_i^A is equal to the radius of corresponding preformed circle shape by N°i axial yarn.

Therefore, the mechanical model during preforming can be set up. According to Coulomb Friction Model, the maximum tension is the reaction force of static friction as yarn sliding occurs instantly. As shown in Fig. 6, the point Q is virtually cut to conveniently analyse the mechanical model of tension. Based on the work presented in [24], the equilibriums can be expressed during the preforming process:

$$\begin{cases} T_e = f_i^A \\ T_m = T_q = T_e e^{\mu_2 \theta_i^A} \\ T_a = T_m e^{\mu_3 \theta_i^A} \end{cases} \tag{2}$$

Where the T_a, T_m, T_q and T_e present the tension at points A, M, Q and E respectively, and f_i^A is the friction of N°i axial yarn generated by upper plate and die. μ_2 and μ_3 symbolize the friction coefficient between yarn and upper plate, yarn and punch tool, respectively.

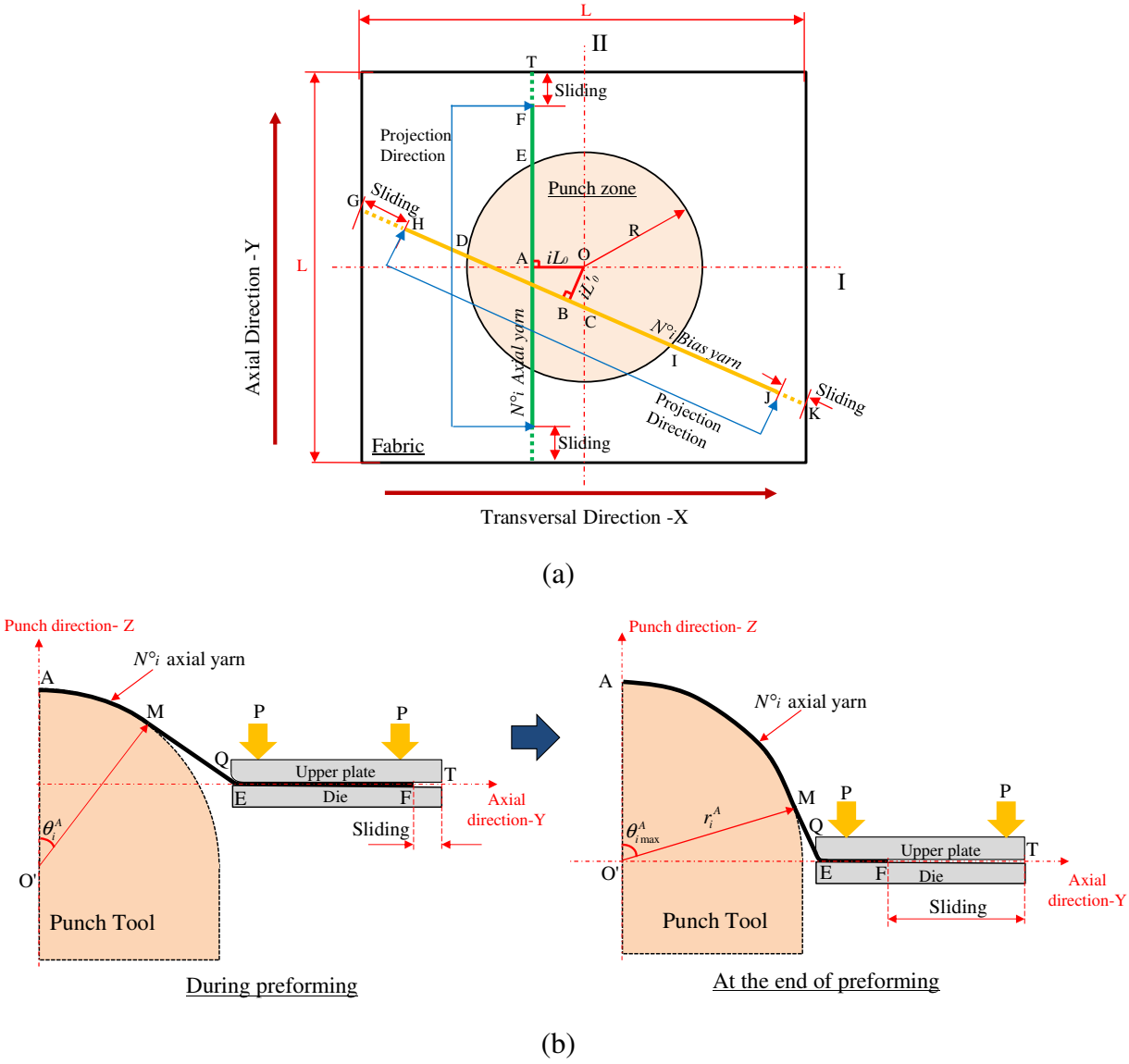

Fig. 5. Sliding occurring during preforming. (a) Geometrical position of N°i axial yarn relative to punch tool, (b) N°i axial yarn formed by the punch.

According to triaxial fabric structure, the crossovers between the upper plate and die, which are the interacting zones made by axial and bias yarns as shown in Fig. 7a, mainly sustain the blank-holder pressure. Hence, the friction condition for axial yarn and bias yarn absolutely shows the difference that needs to be investigated respectively. At first, the area of a crossover section A_x in Fig. 7a can be roughly estimated:

$$A_x = w^2 \sin\beta \tag{3}$$

Where w is the width of yarn. Thus, regarding a body diagram for a segment of crossover shown in Fig. 7b, the equilibriums for top bias yarn in shade zone can be expressed as:

$$\begin{cases} \sigma_a A_x + 2\tau_b S - \sigma_b A_x = 0 \\ \sigma_b A_x = \dfrac{P\left(A - \pi R^2\right)}{n} - \dfrac{T_{qz}}{n_i^A} \end{cases} \tag{4}$$

σ_a and σ_b present the contact stress on axial yarn and top bias yarn, respectively. τ_b is the shear traction that must act along the dashed line in the bias yarn if the yarn were cut there and equilibrium maintained. Both shear and compressive stresses in the bias yarn might contribute to τ_b [25]. S is the area of shear traction and can be calculated by *wd/3*, d is the fabric thickness. P is the blank-holder pressure; A is the fabric area; n is total number of crossovers under the upper plate, which is constant as fixed punch tool; n_i^A denotes the number of crossovers at one end of N°i axial yarn. T_{qz} is component force of T_c in Z direction. The friction generated by one crossover can be explained by:

$$f = 2\mu_1 \sigma_a A_X \tag{5}$$

Where the μ_1 symbolizes the friction coefficient between yarns. Thus, the friction of N°i axial yarn at one end can be expressed by the following:

$$f_i^A = \int_0^{n_i^A} f dx = 2n_i^A \mu_1 \sigma_a A_X \tag{6}$$

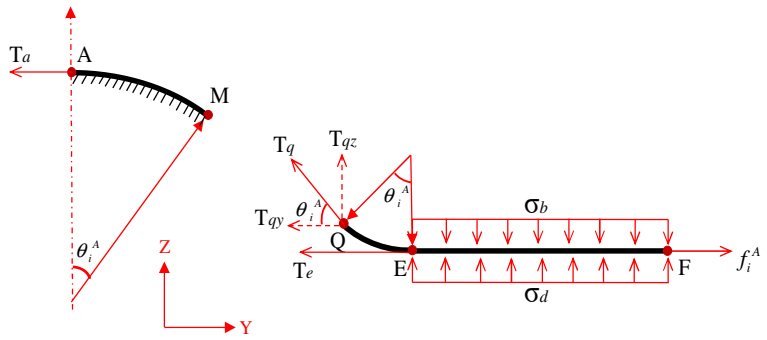

Fig. 6. The schematic diagrams describe the tension generated during the preforming.

If the tension of N°i axial yarn at one end T_i^A can be represented by T_q, it would be deduced according to Eqs. (2-6):

$$T_i^A = T_q = \frac{2n_i^A \mu_1 e^{\mu_2 \theta_i^A} \left(\frac{p\left(A - \pi R^2\right)}{n} - \frac{2}{3} wd\tau_b \right)}{1 + 2\mu_1 e^{\mu_2 \theta_i^A} \sin\theta_i^A} \tag{7}$$

Due to axial yarns symmetrical along I, the tension at two ends is identical because the lengths of the second portion of a yarn that sustains the blank-holder pressure at two ends are equal. Hence, the sliding at the ends for any axial yarn shows identical, yet the sliding degree for different axial yarns is unequal. Besides, due to the identical tension at the ends, the balance is acquired. It means that the first portion of yarn does not move along the punch tool surface.

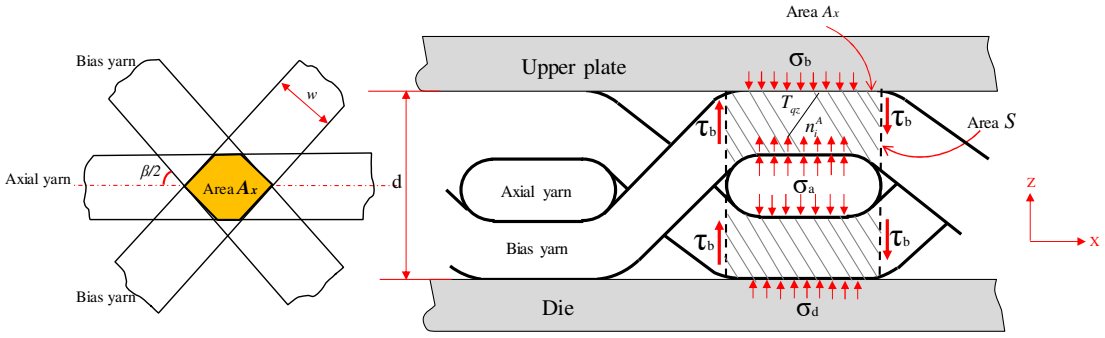

(a) (b)

Fig. 7. The diagram showing load transfer through a crossover region between upper plate and die in theory, (a) the area of crossover and (b) free body diagram in random crossover.

The ideology of analysing the tension of N°i bias yarn (i≠0), T_i^B, is in accordance with T_i^A but it is relatively complicated on the account of two aspects. The first one is that the lengths of the second portion of the yarn, which sustains the blank-holder pressure, are not identical at two ends, as shown in Fig. 5a, $l_{GD} \neq l_{IK}$. Hence, the tension at two ends is also not equal, accordingly generating the difference in sliding. In Fig. 5a, the vertical distance between O point and N°i bias yarn can be fixed and expressed as iL_0' before and after preforming, L_0' is shown in Tab.1. Thus, N°i bias yarn can be projecting into the plane as shown in Fig. 8. The point B is the vertex of corresponding half-circle deformed by N°i bias yarn, and point C is the centre of N°i bias yarn. Indeed, these two points do not coincide resulting in the non-identical sliding at the ends. Moreover, it is deduced that the increasing vertical distance between these two points l_{BC} could aggravate the extent of non-identical sliding at the ends. Therefore, in order to obtain the balance during preforming, the unequal tension at the ends could cause N°i bias yarn to slide on the surface of punch. This is different from N°i axial yarn during preforming. The tension calculation of N°i bias yarn at one end can refer to tension model of N°i axial yarn.

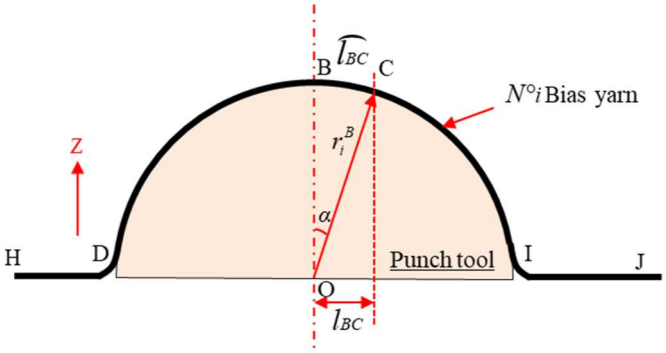

Fig. 8. N°i bias yarn after preforming

Another complicated aspect is about the friction situation. As the braided structure shown in Fig. 7b, the bias yarn alternately locates at top and bottom in two adjacent crossovers, leading to different friction conditions. Thus, the friction calculation at one end of N°i bias yarn, f_i^B, can be roughly expressed as follows:

$$\begin{cases} f_i^B = \dfrac{n_i^B}{2}\left(f_i^t + f_i^b\right) \\ f_i^t = \mu_2\sigma_b A_x + \mu_1\sigma_a A_x \\ f_i^b = \mu_2\sigma_d A_x + \mu_1\sigma_a A_x \end{cases} \tag{8}$$

Where f_i^t and f_i^b stand for the friction forces as N°i bias yarn locates at top and bottom in adjacent crossovers. σ_d is the contact stress on bias yarn at the bottom in shade zone as shown in Fig. 7. Because the upper plate and die are made by the identical material, the μ_2 is friction coefficient in contact surfaces of yarn/upper plate and yarn/die. n_i^B is the number of crossovers at one end under the upper plate. Therefore, the equilibriums in Z-direction can be denoted as:

$$\begin{cases} \sigma_d A_x + 2\tau_b S - \sigma_a A_x = 0 \\ \sigma_a A_x + 2\tau_b S - \sigma_b A_x = 0 \\ \sigma_b A_x = \dfrac{P\left(A - \pi R^2\right)}{n} - \dfrac{T_{qz}}{n_i^B} \end{cases} \tag{9}$$

Based on the derivation of tension for N°i axial yarn, the tension for N°i bias yarn at one end can be expressed as:

$$T_i^B = \frac{n_i^B\left(\mu_1 + \mu_2\right)e^{\mu_2\theta_i^B}\left(\dfrac{p\left(A - \pi R^2\right)}{n} - \dfrac{2}{3}wd\tau_b\right)}{1 + \left(\mu_1 + \mu_2\right)e^{\mu_2\theta_i^B}\sin\theta_i^B} \tag{10}$$

It is suggested from Eqs. (7) and (10) that as fixed punch tool, the tension for N°i bias yarn or axial yarn at one end is heavily associated with the length of the second portion of the yarn and punching displacement. Besides, the punching displacement is inversely proportional to the length of second portion of the yarn, the crossovers are proportional to the length of second portion of the yarn. Especially for bias yarns, in varied braiding angles the punching displacement for N°i bias yarn is different. Thus, the deformability behaviours are changed at magnitude and location as seen in experimental results. On the other hand, the yarns sliding and in-plane shearing are all decided by the yarns tension. It means that the behaviour can be

approximately evaluated through a suitable geometrical model, which is deduced by the punch stroke and the length of the second portion of the yarn.

4.2 The geometrical models of deformability behaviours

As the discussion above, when the tension at the ends reaches the static friction, the sliding occurs instantly. Once the sliding occurs, the friction becomes small. Thus, it is induced from experimental results that the sliding is proportional to punching displacement. However, for different axial and bias yarns, their geometrical position relative to punch zone decides the corresponding punching displacement. Furthermore, the continuous carbon yarn is almost deemed as inextensibility, and after preforming, there is no broken carbon being observed. It is thus suggested that during preforming, once out-of-plane bending starts, the yarns sliding occurs instantly. Therefore, based on the yarns inextensibility before and after preforming, the sliding can be predictably calculated via geometrical analysis. Besides, the sliding also needs to be stated at axial yarns and bias yarns respectively.

4.2.1 The axial yarns sliding

According to Fig. 5a, the half-length of first portion of N°i axial yarn within punch zone, l_{AE}, is geometrically roughly equal to r_i^A after preforming, as shown in Fig. 5b. It means after preforming, the maximum punching displacement r_i^A can be expressed as l_{AE}, which can be conveyed geometrically as follows:

$$r_i^A = l_{AE} = \sqrt{R^2 - \left(iL_0\right)^2} \tag{11}$$

Based on the inextensibility of carbon yarn before and after preforming, the S_i^A, which stands for the anticipated sliding of N°i axial yarn at one end after preforming, can be deduced as follows:

$$\text{Before preforming: } 2S_i^A + 2l_{EF} + l_{AE} = L \tag{12}$$

After preforming: $2l_{EF} + \frac{\pi}{2} r_i^A = L$ (13)

$$S_i^A = \sqrt{R^2 - (iL_0)^2}\left(\frac{\pi}{2} - 1\right) \quad (14)$$

Where L is the width of fabric, $l_{EF}$is the length of second portion of N°i axial yarn under upper plate after preforming. Two general suggestions can be deduced from Eq. (14), firstly, the axial yarns sliding zone can be profiled by semicircle after preforming, which can be proved by the experimental results with braiding angles 55° and 65° as shown in Fig. 4, N°0 axial yarn presents maximum sliding. Secondly, the axial yarns sliding is independent of the braiding angle. Hence, the maximum sliding at one end of axial yarn is almost identical in experimental results with braiding angles 55° and 65° as shown in Fig. 9. If the material draw-in along II line happens, as seen in experimental result with braiding angle 30°, the degree of axial yarns sliding can be restrained by the material draw-in, possibly owing to an augmentation in friction by in-plane shearing of bias yarns. Hence, the relatively low extent of maximum axial yarn sliding is presented by the performance with a braiding angle 30°.

Furthermore, evaluation on the geometrical model should resort to the comparison between theoretical and experimental results of sliding for each axial yarn as shown in Fig. 10, which experimental results are obtained by braiding angles 55° and 65°. It can be suggested that the geometrical model for the sliding of each axial yarn presents good reliability since theoretical and experimental values show a good agreement.

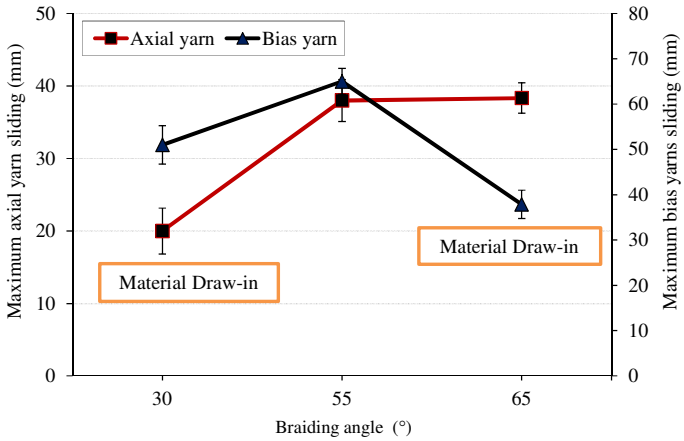

Fig. 9. The maximum yarns sliding varied with different braiding angles.

4.2.2 The bias yarns sliding

As tension discussed above, except the N°0 bias yarn across the centre point of punch zone, the others bias yarns characterize that the tension at the ends is not balanced, the sliding at the ends thus is also not equal. Especially when the difference of the tension at the ends exceeds a certain value, it can be observed during the test that the case which only one end slides but another does not slide occurs. In this case, the maximum sliding at one end of bias yarn in different braiding angles, owing to only one end sliding, can be measured and presented in Fig. 9.

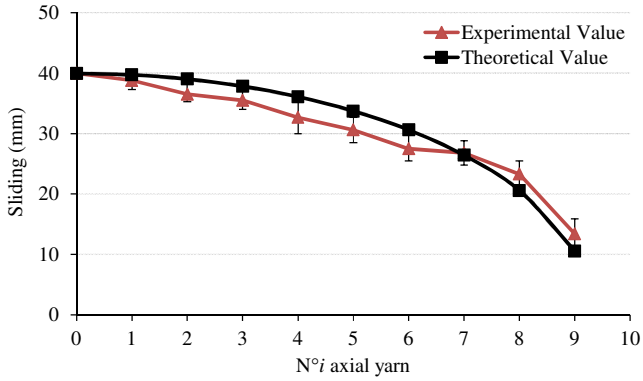

Fig. 10. Comparison of axial yarns sliding between analysed and experimental results.

The geometrical models for two ends of N°i bias yarn can be proposed according to the similar approach with axial yarns. In this section, the geometrical models are only expressed with the braiding angle over 45°. As shown in Fig. 5(a), l_{GK} is the whole length of N°i bias

yarn before preforming. After preforming, uneven sliding at the ends is accordingly anticipated and can be represented by l_{GH} and l_{JK}, which can be expressed as follows:

$$\text{Before preforming: } l_{GH} + l_{HD} + l_{DC} = \frac{l_{GK}}{2} \tag{15}$$

$$\text{After preforming: } l_{HD} + \widehat{l}_{DB} + \widehat{l}_{BC} = \frac{l_{GK}}{2} \tag{16}$$

$$S_{Left}^{B} = l_{GH} = \widehat{l}_{DC} - l_{DC} \tag{17}$$

Where S_{Left}^{B} stands for the sliding at the left end l_{GH}. The S_{Right}^{B} that represents the sliding at the right end l_{JK}, can be determined as the same way:

$$\text{Before preforming: } l_{CI} + l_{IJ} + l_{JK} = \frac{l_{GK}}{2} \tag{18}$$

$$\text{After preforming: } \widehat{l}_{CI} + l_{IJ} = \frac{l_{GK}}{2} \tag{19}$$

$$S_{Right}^{B} = l_{JK} = \widehat{l}_{CI} - l_{CI} \tag{20}$$

It is directly suggested from the Eq. (17) and (20) that the sliding at the ends is no longer identical. Based on Fig. 8, the punching displacement for N°i bias yarn after preforming is equal to the radius of the ideally punched circle by corresponding yarn, r_i^B, which is half of the length of segmental N°i bias yarn within punch zone l_{DI}, as shown in Fig. 5.

$$r_i^B = \frac{l_{DI}}{2} = \sqrt{R^2 - \left(iL_0'\right)^2} \tag{21}$$

l_{BC} is the vertical distance between two points B and C, and its corresponding arc length, $\widehat{l}_{BC}$, and angle α after preforming can be expressed according to Fig. 8:

$$\begin{cases} l_{BC} = \dfrac{iL_0'}{\tan\left(\dfrac{\beta}{2}\right)} \\ \alpha = \arcsin\left(\dfrac{l_{BC}}{r_i^B}\right) = \arcsin\left[iL_0' \Big/ \tan\left(\dfrac{\beta}{2}\right)\sqrt{R^2 - \left(iL_0'\right)^2} \right] \\ \widehat{l}_{BC} = \alpha r_i^B = \arcsin\left[iL_0' \Big/ \left(\tan\left(\dfrac{\beta}{2}\right)\sqrt{R^2 - \left(iL_0'\right)^2} \right) \right] \sqrt{R^2 - \left(iL_0'\right)^2} \end{cases} \tag{22}$$

Therefore, the difference of sliding at the ends S_d after preforming can be defined as:

$$\begin{cases} S_d = S_{Left}^B - S_{Right}^B = 2\left(\widehat{l}_{BC} - l_{BC}\right) \\ S_d = 2\left(\arcsin\left[iL_0' \Big/ \left(\tan\left(\frac{\beta}{2}\right)\sqrt{R^2 - \left(iL_0'\right)^2} \right) \right] \sqrt{R^2 - \left(iL_0'\right)^2} - \frac{iL_0'}{\tan\left(\frac{\beta}{2}\right)} \right) \end{cases} \tag{23}$$

S_d directly stands for the sliding difference at two ends, meaning the extent of different tension between two ends. It is clearly deduced that the tension difference at the ends is heavily associated with the braiding angle as the fixed diameter of the punch. Increasing S_d denotes that the unbalanced tension at two ends is aggravated. Besides, the maximum sliding at one end of bias yarn is positively related to S_d. In the same way, when the braiding angle below 45°, S_d can be expressed as follows:

$$S_d = 2\left(\arcsin\left[\tan\left(\frac{\beta}{2}\right)\left(iL_0'\right) \Big/ \sqrt{R^2 - \left(iL_0'\right)^2} \right] \sqrt{R^2 - \left(iL_0'\right)^2} - \tan\left(\frac{\beta}{2}\right)\left(iL_0'\right) \right) \tag{24}$$

Fig. 11 shows the relation between S_d and braiding angles for each numbered bias yarn based on Eq. (23). It is suggested that, in theory, S_d increases as continually numbered bias yarns (from N°0 to N°i) when braiding angle is fixed, meaning that the unbalance of tension at the ends is aggravated. The case that only one end slides but another does not slide would start to appear as S_d is large enough. It is dominated by the work induced by the tension difference between the two ends. Moreover, S_d increased as continually numbered bias yarns does not mean that the degree of only one end sliding always show a rising trend. This is because with continually numbered bias yarns, the corresponding punching displacement decreases and therefore sliding decreases accordingly. Hence, the bias yarns sliding zones can be likely profiled as parabola shown in experimental results (Figs. 4b and 4c).

Furthermore, as shown in Fig. 11, it is also clearly seen that S_d for each bias yarn increases from braiding angle 0° to 45°, decreases from 45° to 90°, and is symmetrical at braiding angle

45°. Besides, as fixed N°i bias yarn, S_d at braiding angle 55° shows the larger value than S_d at 30° and 65°. It means that the maximum sliding at braiding angle 55° shows relatively larger value than other braiding angles, which can be proved by the experimental results as shown in Fig. 9.

On the other hand, the model for N°i bias yarn sliding at one end is also proposed based on Eqs. (15-22) as follows, for example S_{Right}^{B}.

$$S_{Right}^{B}=\frac{\pi\sqrt{R^2-\left(iL_0'\right)^2}}{2}-\arcsin\left[iL_0'\Big/\left(\tan\left(\frac{\beta}{2}\right)\sqrt{R^2-\left(iL_0'\right)^2}\right)\right]\sqrt{R^2-\left(iL_0'\right)^2}-\sqrt{R^2-\left(iL_0'\right)^2}+\frac{iL_0'}{\tan\left(\frac{\beta}{2}\right)} \tag{25}$$

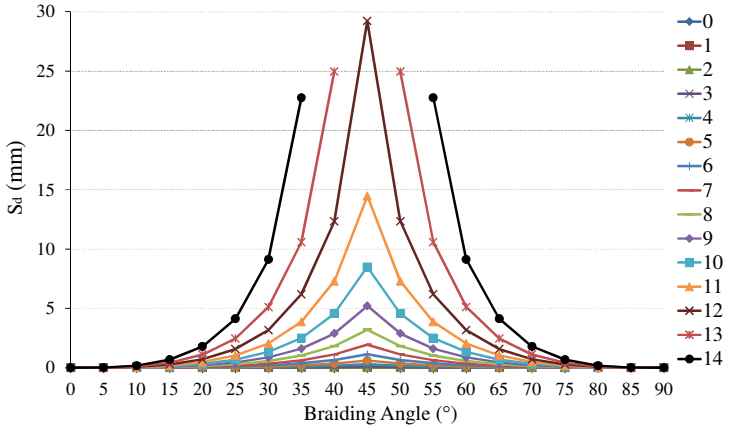

Fig. 11. The sliding difference S_d between the ends for each bias yarn varied with different braiding angles.

Fig. 12 shows the comparison between experimental results and S_{Right}^{B}. It is believed that this model is partly able to predict sliding of each bias yarn at one end. The sliding in first six bias yarns in experimental results shows a relatively good agreement with the theoretical value. It can be deemed as pure sliding because the degree of tension difference between two ends could not heavily influence the sliding. However, from N°7 bias yarn, the large tension difference between two ends produces that the case which only end slides but another does not slide occurs, thus the sliding at one end suddenly becomes almost zero. This is because bias yarns show the tension difference between two ends, leading to unbalance between two

ends during the tests. Thus, the work would be induced by this case in order to achieve the balance between two ends, leading to bias yarns sliding on the punch tool surface. When the extent of tension difference (S_d) beyond a certain value, only one end sliding would occur. Therefore, the sliding at one end in experimental data shows such drastically jumping. However, it exceeds the prediction ability of geometrical analysis on sliding because the geometric models are only according to the geometrical position before and after preforming without considering the work induced by unequal tension at two ends. The experimental result of braiding angle 30° also shows this case, but which numbered bias yarn starts doing this case is different from braiding angle 55° and 65°. This is because S_d is different among these braiding angles as fixed N°i bias yarn, expressing that the numbered bias yarn which starts to present only one end sliding is varied. Unfortunately, this geometric model cannot predict which one yarn starts doing this case.

In comparison to theoretical and experimental values for axial and bias yarns, it can be concluded that the geometrical analysis on sliding is more adaptable for axial yarns since the tension at two ends is equal, so the balance at the ends could be achieved during the preforming.

4.2.3 In-plane shearing and material draw-in

As shown in experimental results, the in-plane shearing or material draw-in takes place along I or II line out of punch zone. In theory, the interlaced bias yarns inclining to in-plane shear must respect the law that the bias yarns should sustain the identical tension at the crosspoints. It means that only the interlaced bias yarns whose crosspoints approximately locate at the I or II line are prone to in-plane shear. This is because the lengths of second portion for interlaced bias yarns under upper plate are equal, generating the identical tension of interlaced bias yarns at the crosspoints, as shown in Fig. 13. The in-plane shearing impels

the interlaced bias yarns to rotate towards each other, as classical definition of shearing angle γ shown in Fig. 1b, the in-plane shearing zones along I line thus show a negative value of the in-plane shearing angle. Other interlaced bias yarns whose cross-points do not locate at the I or II line tend to slide rather than in-plane shear theoretically due to uneven tension at crosspoints.

Provided that one crosspoint almost coincides with the intersection of the boundary of punch zone and the II line, as shown in Fig. 13, the maximum length on the left side of this cross-point can be geometrically defined as l_0. In this case, l_n stands for length on the left side of other crosspoints locating at the II line from the boundary of punch zone to fabric border. It is evidently shown that l_n presents the descending tendency, leading to a decreasing tension at continuous crosspoints along the II line. Accordingly, the degree of in-plane shearing would also show this tendency. Similarly, the in-plane shearing occurring along the I line would also show the same tendency as the II line.

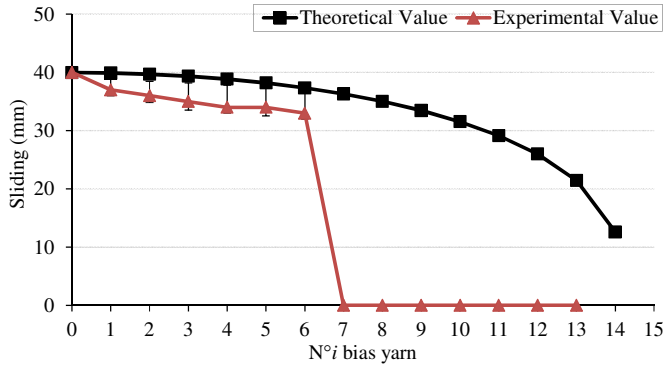

(a)

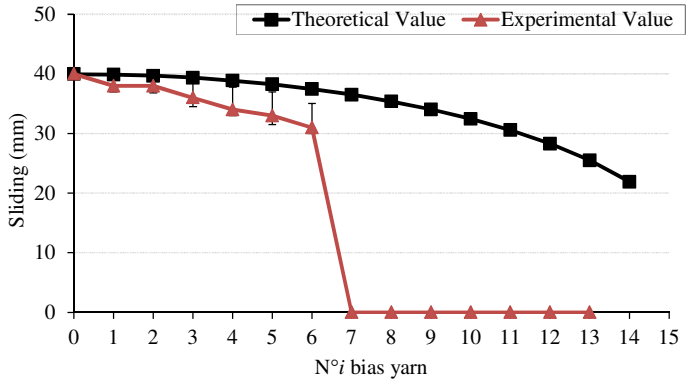

(b)

Fig. 12. The comparison between the theoretical and experimental value of sliding for each bias yarn; (a) braiding angle 55°, (b) braiding angle 65°.

The in-plane shearing angle measured after preforming can be used to verify this prediction as shown in Fig. 14, which depicts the in-plane shearing angle variation at braiding angle 55° from the base of the punch zone to fabric border, where can be divided into three zones after preforming (zones 1-3), as shown in Fig. 4. The small in-plane shearing angle presents the corresponding small degree of in-plane shearing. It is thus concluded that the degree of in-plane shearing decreases along I or II line from the base of punch zone to the fabric border.

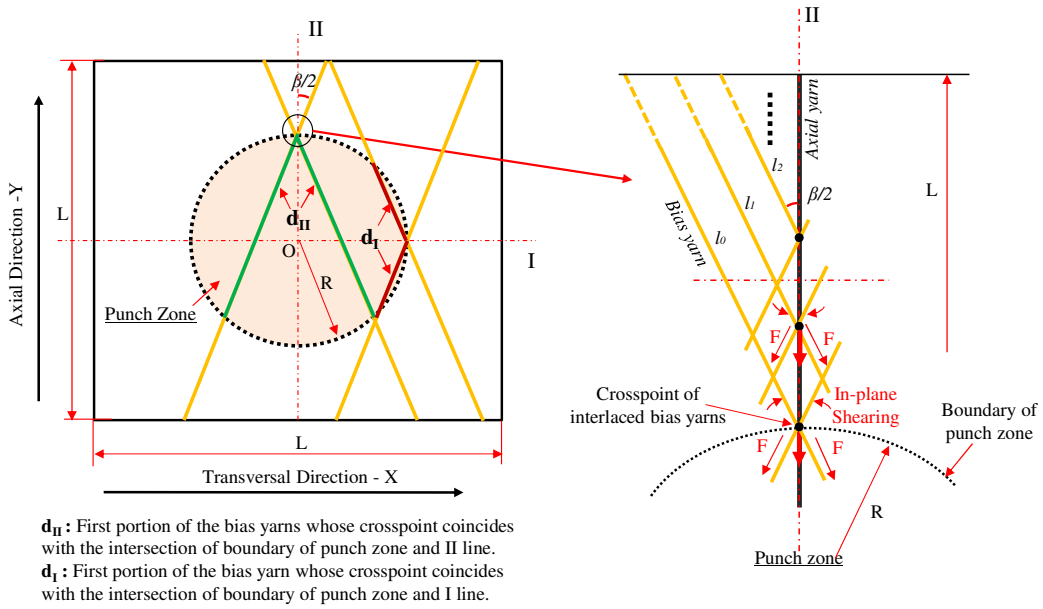

Fig. 13. The 2D diagram to describe in-plane shearing during preforming.

From another perspective, l_0 shown in Fig. 13 is inversely proportional to the corresponding length of first portion of the yarn along the II line, which can be symbolized as d_{II}. It implies that d_{II} can directly reflect the maximum degree of in-plane shearing along the II line. Similarly, d_I can be also geometrically defined along the I line. Thus, under the fixed braiding angle, which line would show the more visible in-plane shearing could be predictable directly to make a comparison between d_{II} and d_I. The d_{II} and d_I are expressed as follows:

$$d_{II} = 2R\cos\left(\frac{\beta}{2}\right) \tag{26}$$

$$d_{I} = 2R\sin\left(\frac{\beta}{2}\right) \tag{27}$$

It is clearly seen that d_{II} and d_I are decided by the braiding angle, meaning that the variation of degree and location of in-plane shearing in different braiding angles (seen in Fig. 4) can be explained by comparing the difference between d_{II} and d_I. As shown in Fig. 15a, when the braiding angle is equal to 45°, $d_{II} = d_I$, the second portions of bias yarn at the ends are same, the tension at the ends is thus almost identical so that the in-plane shearing or material draw-in shows the same extent with symmetrical distribution at the fabrics. It can account for the characteristic of the in-plane shearing in woven fabric preforming [2,22]. When the braiding angle descends from 45° gradually as shown in Fig. 15b, $d_{II} > d_I$, d_{II} and d_I become uneven, denoting that the degree of in-plane shearing along the II line turns to be large. This is because l_n along the II line becomes short, the friction becomes small, and consequently, the in-plane shearing is more prone to occur along the II line. By contrast, l_n along the I line increases, the degree of in-plane shearing along the I line gradually becomes small since the friction increases so that in-plane shearing is no longer easy to happen.

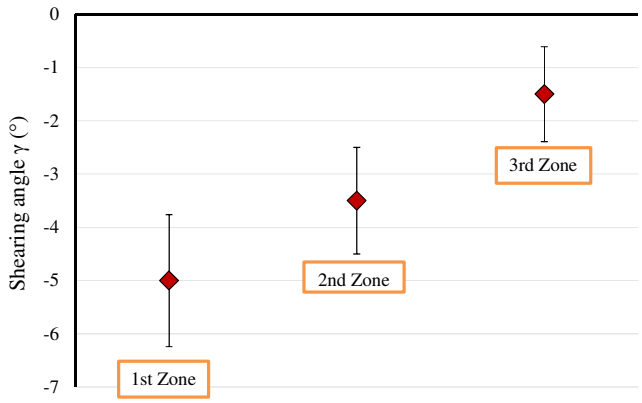

Fig. 14. The variation of the in-plane shearing angle at braiding angle 55°.

As braiding angle descends further, material draw-in along the II line would take place. This is because when bias yarns occurring in-plane shearing approach the "locking angle" [8],

the stage of in-plane shearing would finish and then the sliding at the end will happen. Meanwhile, the in-plane shearing along with the I line probably disappears because the friction is too large to generate in-plane shearing, the experimental results shown in Fig. 4a can confirm this inference. Conversely, when increasing the braiding angle from 45° as shown in Figs. 15c and 15d, $d_{II} < d_I$, the appearance of in-plane shearing and material draw-in along the I line shows the similar trend with decreasing braiding angle from 45°, and can be verified by the experimental results in braiding angle 55° and 65°, as shown in Figs. 4b and 4c. The in-plane shearing angle γ measured after preforming tests can be deemed as a character to verify this variation as shown in Fig. 16. The positive or negative in-plane shearing angle γ shows the in-plane shearing or even material draw-in takes place along the II or I line, respectively. It is clearly suggested from Fig. 16 that as increasing the braiding angle the difference between d_{II} and d_I varies, besides the in-plane shearing location is also varied. The material draw-in would possibly occur as enlarging the difference between d_{II} and d_I. Therefore, by resort to braiding angle and diameter of punch tool, the in-plane shearing or even material draw-in could be predictable with respect to degree and location.

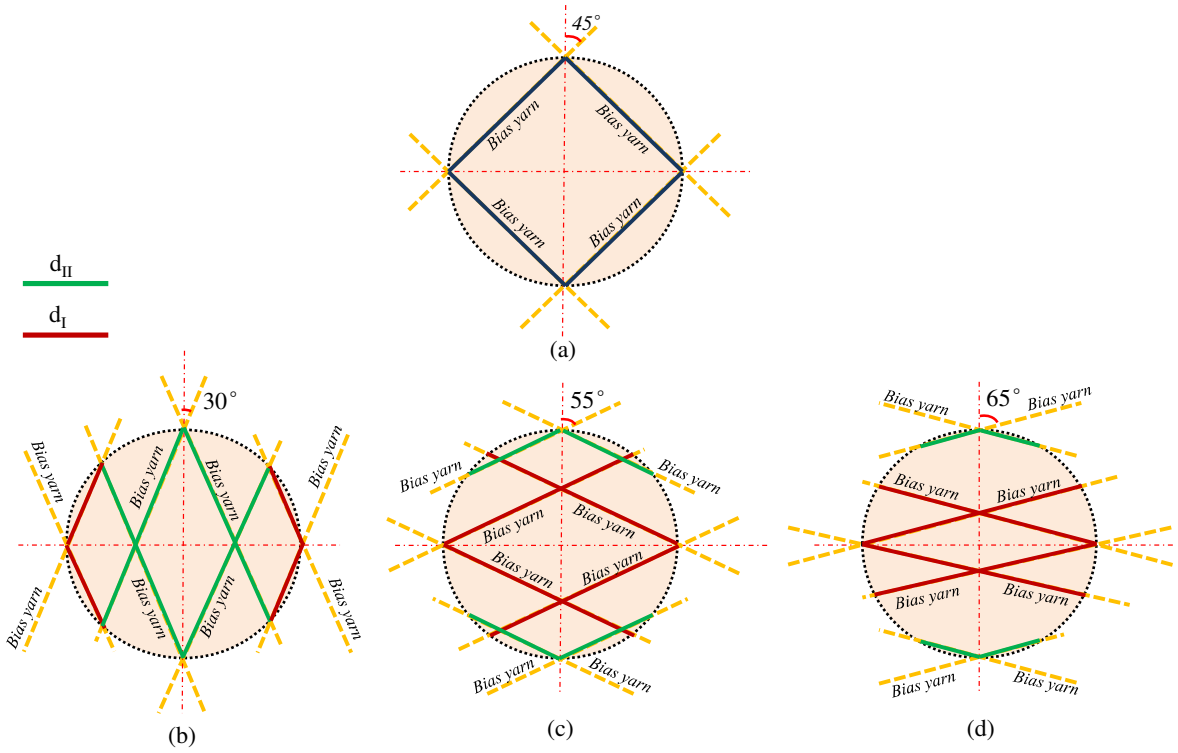

Fig. 15. The change of segmental yarn length in punch shape with different braiding angles; (a) $\beta/2$=45°, (b) $\beta_0/2$=30°, (c) $\beta_1/2$=55°and (d) $\beta_2/2$=65°.

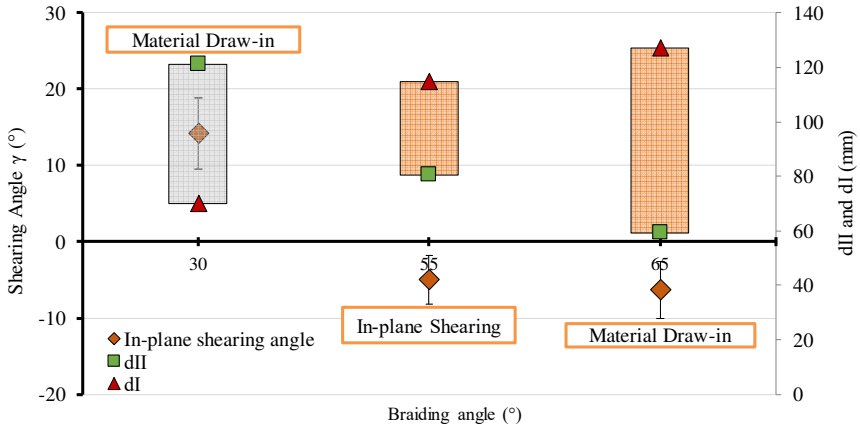

Fig. 16. The variation of in-plane shearing angle with different braiding angles.

5. Conclusion

The triaxial fabrics as promising reinforcements for advanced composite manufacturing were originally investigated during preforming process with respect to deformability behaviours such as in-plane shearing and yarns sliding based on varied braiding angles by virtue of mechanical and experiment analysis. Firstly, the tension model for yarn was proposed based on parameters of triaxial fabrics and punch tool in order to understand the driven force for deformability behaviours. It is suggested from the models that the braiding angle directly impacted the tension of the yarn generated during preforming. Secondly, based on the inextensibility of continuous carbon yarn, the geometrical models for yarns sliding were expressed and verified in order to precisely describe the yarns sliding. It is clearly seen that varying braiding angle visually affected the degree of in-plane shearing as shown in experimental results. Axial yarns sliding, presenting identical sliding at the ends, showed a good agreement between the model and experimental results of sliding for each axial yarn. However, the bias yarn sliding was relatively complicated. This is because the uneven tension generated at the ends produced unequal sliding. The geometrical model partly described the sliding of bias yarns. At last, in-plane shearing or even material draw-in only occurred along

the central line of punch tool (I or II line), which locates at axial and transversal directions of fabric, and its degree decreased from base of punch zone to fabric border. Besides, in-plane shearing or material draw-in could be predicted through comparing the length of portion yarn within punch zone. When the length of portion yarn along the II line is larger than that along the I line, the in-plane shearing phenomenon relatively shows more obvious along the II line. Conversely, the in-plane shearing is more visible along the I line.

Therefore, the conclusion can be drawn that the braiding angle greatly impacted the variation of deformability behaviours, which can be geometrically predicted at the perspectives of degree and tendency before preforming.

Acknowledgement

The authors gratefully appreciate the financial support from the China Scholarship Council (CSC)

Reference

[1] Baran I. Advances in Composites Manufacturing and Process Design. Woodhead Publishing Series in Composites Science and Engineering; 2015. https://doi.org/10.1016/B978-1-78242-307-2.00016-6.

[2] Xiao S, Wang P, Soulat D, Legrand X, Gao H. Towards the deformability of triaxial braided composite reinforcement during manufacturing. Compos Part B Eng 2019;169:209–20. https://doi.org/10.1016/J.COMPOSITESB.2019.04.017.

[3] Ouagne P, Soulat D, Moothoo J, Capelle E, Gueret S. Complex shape forming of a flax woven fabric; Analysis of the tow buckling and misalignment defect. Compos Part A Appl Sci Manuf 2013;51:1–10. https://doi.org/10.1016/j.compositesa.2013.03.017.

[4] Mouritz AP, Bannister MK, Falzon PJ, Leong KH. Review of applications for advanced three-dimensional fibre textile composites. Compos Part A Appl Sci Manuf 1999;30:1445–61. https://doi.org/10.1016/S1359-835X(99)00034-2.

[5] Liao T, Adanur S. 3D Structural Simulation of Tubular Braided Fabrics for Net-Shape Composites. Text Res J 2000;70:297–303. https://doi.org/10.1177/004051750007000403.

[6] Kyosev Y. Topology-Based Modeling of Textile Structures and Their Joint Assemblies. Springer International Publishing; 2019. https://doi.org/10.1007/978-3-030-02541-0.

[7] Xiao S, Lanceron C, Wang P, Soulat D, Gao H. Mechanical and thermal behaviors of ultra-high molecular weight polyethylene triaxial braids: the influence of structural parameters. Text Res J 2018:004051751881194. https://doi.org/10.1177/0040517518811944.

[8] Xiao S, Wang P, Soulat D, Minet J, Zemni L, Gao H. Analysis of the in-plane shear behaviour of non-orthogonally textile reinforcements: Application to braided fabrics.

Compos Part B Eng 2018;153:159–66. https://doi.org/10.1016/J.COMPOSITESB.2018.07.040.
[9] Potluri P, Manan A. Mechanics of non-orthogonally interlaced textile composites. Compos Part A Appl Sci Manuf 2007;38:1216–26. https://doi.org/10.1016/j.compositesa.2006.04.008.
[10] Sharma SB, Sutcliffe MPF, Chang SH. Characterisation of material properties for draping of dry woven composite material. Compos Part A Appl Sci Manuf 2003;34:1167–75. https://doi.org/10.1016/j.compositesa.2003.09.001.
[11] Ouagne P, Soulat D, Hivet G, Allaoui S, Duriatti D. Analysis of defects during the preforming of a woven flax reinforcement. Adv Compos Lett 2011;20:105–8.
[12] Sjölander J, Hallander P, Åkermo M. Forming induced wrinkling of composite laminates: A numerical study on wrinkling mechanisms. Compos Part A Appl Sci Manuf 2016;81:41–51. https://doi.org/10.1016/j.compositesa.2015.10.012.
[13] Hamila N, Boisse P, Sabourin F, Brunet M. A semi-discrete shell finite element for textile composite reinforcement forming simulation. Int J Numer Methods Eng 2009;79:1443–66. https://doi.org/10.1002/nme.2625.
[14] Gereke T, Döbrich O, Hübner M, Cherif C. Experimental and computational composite textile reinforcement forming: A review. Compos Part A Appl Sci Manuf 2013;46:1–10. https://doi.org/10.1016/j.compositesa.2012.10.004.
[15] Khan MA, Mabrouki T, Vidal-Sallé E, Boisse P. Numerical and experimental analyses of woven composite reinforcement forming using a hypoelastic behaviour. Application to the double dome benchmark. J Mater Process Technol 2010;210:378–88. https://doi.org/10.1016/j.jmatprotec.2009.09.027.
[16] Jacquot PB, Wang P, Soulat D, Legrand X. Analysis of the preforming behaviour of the braided and woven flax/polyamide fabrics. J Ind Text 2016;46:698–718. https://doi.org/10.1177/1528083715591592.
[17] Gatouillat S, Bareggi A, Vidal-Sallé E, Boisse P. Meso modelling for composite preform shaping - Simulation of the loss of cohesion of the woven fibre network. Compos Part A Appl Sci Manuf 2013;54:135–44. https://doi.org/10.1016/j.compositesa.2013.07.010.
[18] Zhu B, Yu T, Zhang H, Engineering XT-CPB, 2011 U. Experimental investigation of formability of commingled woven composite preform in stamping operation. Compos Part B Eng 2011;42:289–95.
[19] Gao Y, Li J. Effects of braiding angle on modal experimental analysis of three-dimensional and five-directional braided composites. Compos Part B Eng 2012;43:2423–8. https://doi.org/10.1016/J.COMPOSITESB.2011.11.025.
[20] Okano M, Sugimoto K, Saito H, Nakai A, Hamada H. Effect of the braiding angle on the energy absorption properties of a hybrid braided FRP tube. Proc Inst Mech Eng Part L J Mater Des Appl 2005;219:59–66. https://doi.org/10.1243/146442005X10256.
[21] Tate JS, Kelkar AD, Whitcomb JD. Effect of braid angle on fatigue performance of biaxial braided composites. Int J Fatigue 2006;28:1239–47. https://doi.org/10.1016/J.IJFATIGUE.2006.02.009.
[22] Labanieh AR, Garnier C, Ouagne P, Dalverny O, Soulat D. Intra-ply yarn sliding defect in hemisphere preforming of a woven preform. Compos Part A Appl Sci Manuf 2018;107:432–46. https://doi.org/10.1016/j.compositesa.2018.01.018.
[23] Lo WM, Hu JL. Shear Properties of Woven Fabrics in Various Directions. Text Res J 2002;72:383–90. https://doi.org/10.1177/004051750207200502.
[24] Marciniak Z, Duncan JL, Hu SJ. Mechanics of sheet metal forming. Butterworth-Heinemann; 2002.

[25] Ruggy KL, Cox BN. Deformation Mechanisms of Dry Textile Preforms under Mixed Compressive and Shear Loading. J Reinf Plast Compos 2004;23:1425–42. https://doi.org/10.1177/0731684404039779